Journal of Materials Chemistry

Cite this: *J. Mater. Chem.*, 2012, **22**, 16066

www.rsc.org/materials

PAPER

Biocompatible fluorescent core–shell nanoparticles for ratiometric oxygen sensing†

Xiao-Hui Wang,[a] Hong-Shang Peng,*[a] He Ding,[a] Fang-Tian You,[a] Shi-Hua Huang,[a] Feng Teng,[a] Biao Dong[b] and Hong-Wei Song[b]

Received 5th April 2012, Accepted 18th June 2012
DOI: 10.1039/c2jm32122j

Ratiometric fluorescent core–shell nanoparticles (NPs) with good biocompatibility are successfully prepared by a one-step reprecipitation–encapsulation method for sensing dissolved oxygen. The particle core comprises the oxygen probe platinum(II) octaethylporphine (PtOEP), the reference dye coumarin 6 (C6) and a third fluorophore dinaphthoylmethane (DNM). Upon single 381 nm excitation, C6 gives oxygen-insensitive referenced green fluorescence *via* intraparticle FRET from DNM, whilst PtOEP yields highly oxygen-sensitive red phosphorescence with a quenching response of 94%. The fluorescence quenching of the NPs against oxygen follows a linear Stern–Volmer behavior, which is fundamental for practical sensing. Moreover, positively charged poly-L-lysine molecules are *in situ* self-assembled onto the surface of NPs during synthesis. The resultant core–shell NPs with functional groups exhibit low cytotoxic effects as well as effortless cellular uptake, indicating targeted intracellular oxygen sensing is very promising using the oxygen nanosensors.

1. Introduction

Measuring and imaging dissolved oxygen in living cells is of major importance, since cellular oxygen levels are closely related to various physiological and pathological processes.[1–4] In terms of *in vivo* oxygen sensing, phosphorescent transition-metal complex sensors are very attractive with their highly sensitive ^{3}MLCT (metal-to-ligand charge transfer) emitting state.[5,6] By measuring their lifetimes using, for example, microsecond fluorescence-lifetime imaging microscopy, accurate assessment of intracellular oxygen has been performed.[7] Unfortunately, such lifetime-based modalities are not as popular and/or convenient as intensity-based measurements.[8] Because single-intensity-based sensing can not give quantitative information unless in cases where the precise concentration of the probes is known, more robust signals are obtained by ratiometric approaches, *i.e.* simultaneously detecting two signals by a single excitation wavelength.[9] Significant efforts have been dedicated to the development of ratiometric oxygen sensors up to now. Aside from chemical synthesis of sensor molecules,[10] most ratiometric oxygen sensors are designed by incorporating reference–probe dual-dye systems into an inert matrix in the form of sensor strips,[11] films,[12] microparticles[13] and nanoparticles (NPs).[14–19] These reference–probe dyes necessarily are either related by fluorescence resonance energy transfer (FRET) or overlap well in their absorption spectra, so that two signals can be rendered under single-wavelength excitation. However, the number of dual-dye systems is limited by the stringent requirement in spectra. Reference–probe dyes that are not matched in spectra, though abundant, rarely find applications in ratiometric nanosensors. The challenge lies in the undermined sensitivity by requiring two-wavelength excitation towards the respective dye, which is subject to drifts of the optoelectronic system.

In this work, we present a first example of a ratiometric core–shell fluorescent oxygen nanosensor, prepared from spectrally non-matched reference–probe dyes, with single-wavelength excitation. Specifically, the fluorescent sensor particle comprises the oxygen probe platinum(II) octaethylporphine (PtOEP), the reference dye coumarin 6 (C6) and the third fluorophore dinaphthoylmethane (DNM). Upon single excitation, PtOEP yields oxygen-sensitive red phosphorescence, whilst DNM transfers the excitation to C6 and consequently results in referenced green fluorescence. The intensity ratio of the dual-fluorescence is highly sensitive to dissolved oxygen. Moreover, the sensing NPs are *in situ* modified with bio-molecules during particle synthesis. The resultant core–shell structured NPs exhibit very low cytotoxic effects and can be effortlessly introduced into living cells. These salient features such as high sensitivity, nanoscale dimension, ratiometric emission as well as good biocompatibility make the NPs superior sensors for intracellular oxygen.

[a]*Key Laboratory of Luminescence and Optical Information, Ministry of Education, Institute of Optoelectronic Technology, Beijing Jiaotong University, Beijing 100044, China. E-mail: hshpeng@bjtu.edu.cn*
[b]*State Key Laboratory on Integrated Optoelectronics, College of Electronic Science and Engineering, Jilin University, Changchun 130012, China*
† Electronic supplementary information (ESI) available: DSL, SEM and excitation spectrum of sensing NPs. See DOI: 10.1039/c2jm32122j

2. Results and discussion

2.1. Synthesis and characterization of core–shell sensing NPs

The core–shell ratiometric sensing NPs are prepared by a modified encapsulation–reprecipitation (ER) method.[20,21] Details are given in the Experimental section. Briefly, a THF solution of polystyrene (PS), dodecyltrimethoxysilane (DTS) and three fluorophores is injected into basic water containing poly-L-lysine (PLL). PS and DTS respectively function as matrix and silica-based encapsulation agent. Positively charged PLL is introduced as a bio-modification agent to adjust the surface charge of the NPs. As a result of the sudden increase in the water/THF ratio, these hydrophobic species aggregate to form particles (stage 1 in Fig. 1(A)). Meanwhile, base-catalyzed hydrolysis and condensation of DTS lead to the silica-based encapsulation of particles. PLL molecules are subsequently adsorbed onto the particle surface by electrostatic forces between amino and silanol groups, and surface modification is thus *in situ* accomplished (stage 2). The resultant NPs are of a core–shell structure, as schematically depicted in Fig. 1(B). The three fluorophore dopants are randomly entrapped in a hydrophobic hybrid core (DTS–PS) encapsulated by negatively charged silica layer, which is further covered with a layer of PLL.

The NP morphology is analyzed by transmission electronic microscope (TEM) and scanning electron microscope (SEM). TEM images in Fig. 1(C) clearly show the presence of an outer layer around the particle core, indicating the success of PLL coating. From the SEM images it can be seen that the core–shell NPs are spherical with an average diameter of 130 ± 50 nm (Fig. 1(D) and (E)), which is consistent with the hydrodynamic size obtained from a Zetasizer analyzer (~120 nm, Fig. S1 in ESI†). The NPs are well dispersed in the dried states, proposed to result from the protection of the PLL shell. In contrast, primary C6–DNM–PtOEP NPs without a PLL coating are found to be seriously aggregated (Fig. S2a†). The existence of the PLL shell is also verified by the significant increase of zeta potential of the NPs from −37.4 mV (primary NPs, Fig. S2b†) to 45.5 mV (NPs with PLL coating, Fig. S2c†). The positive net charge is favorable for the NPs to interact with negative cell membrane and thereafter cellular uptake. Moreover, PLL layers on the NPs surface are helpful to resist adsorption of proteins, which is important for intracellular sensing.[22]

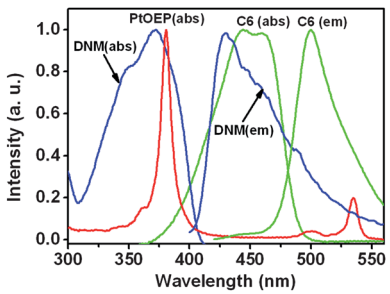

Fig. 2 Spectral properties of C6, DNM and PtOEP in THF solution. DNM and C6 are excited with 381 nm and 450 nm light respectively.

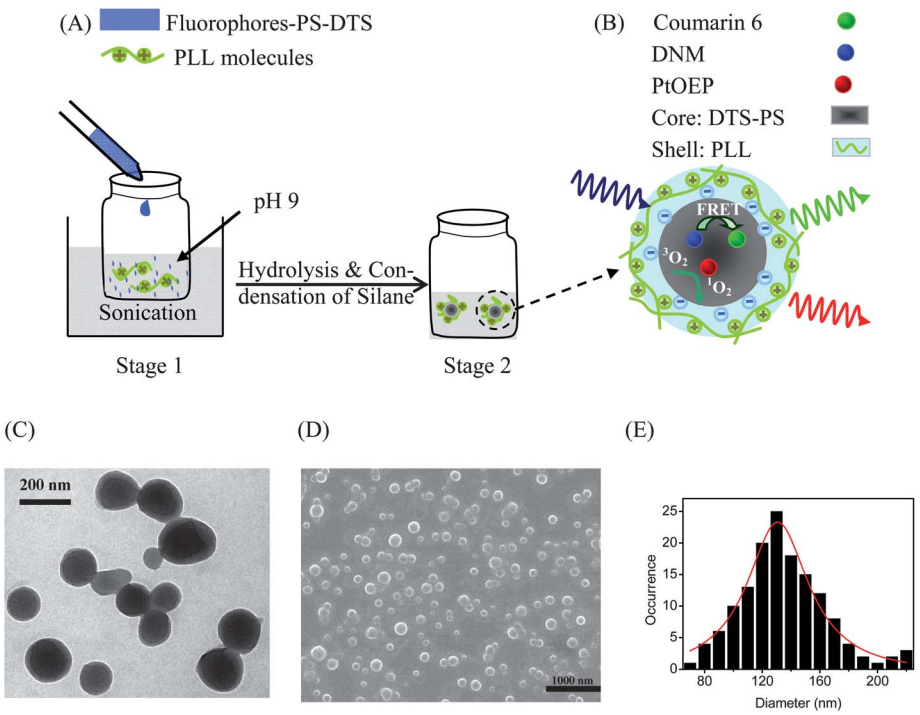

Fig. 1 Ratiometric core–shell sensing NPs. (A) Schematic representation of the synthesis. Electrostatic attraction between amino and silanol groups enables the PLL modification. (B) Model of cross-section. The three fluorophore dopants are confined within the nanosale core (composed of DTS–PS), which is covered first by a silica layer and then a PLL layer. (C) Representative TEM and (D) SEM images. (E) Histogram of diameter data obtained from the SEM image in (D).

2.2. Spectral properties of core–shell sensing NPs

Ratiometric sensing capability of the C6–DNM–PtOEP NPs depends on the spectral relationship of the three dyes. As shown in Fig. 2, the intense Soret band of PtOEP (at 381 nm) has few overlaps with the absorption of C6, *i.e.* the 381 nm excitation on the probe is inefficient for the reference. The fluorophore DNM, previously employed as ligands to nonradiatively transfer excitation energy to europium ions,[21,23] is utilized herein to match the discrepancy in excitation. Its absorption covers that of PtOEP, and emission coincides with the absorption of C6. Therefore, dual fluorescence is expected from the C6–DNM–PtOEP architecture with a single excitation: PtOEP is directly excited to give red phosphorescence, while C6 is indirectly excited *via* intraparticle FRET, from DNM to C6, to give referenced green fluorescence (illustrated in Fig. 1(B)).

The aqueous dispersions of the resultant NPs are transparent, with a light yellow color derived from the absorption of fluorophore dopants. As expected, the ratiometric NPs exhibit dual emission under single excitation (Fig. 3). The two peaks at 490 and 645 nm are assigned to C6 and PtOEP, respectively. To further elucidate the function of DNM, three model hybrid NPs are prepared as well. The first (model NP-1) contains C6 and PtOEP only, the second (model NP-2) contains DNM and PtOEP only, and the third (model NP-3) contains PtOEP only. The concentration of PtOEP, C6 and DNM is kept constantly at 1 wt%, 3 wt% and 3 wt% in respective NPs. With the absence of DNM, the green emission of C6 is weak in model NP-1 – a consequence of inefficient excitation (Fig. 3); however, DNM does not contribute to the green emission directly, as is demonstrated by its weak blue emission around 440 nm in model NP-2. In addition, it is noticed that the red phosphorescence in C6–DNM–PtOEP NPs is considerably enhanced in comparison with that in the three model NPs. The enhancement is investigated by inspection of its excitation spectrum (Fig. S3†), and justified by a two-step FRET. Energy is first transferred from DNM to C6, and then partially from C6 to PtOEP.

2.3. Oxygen sensitivity of the sensing NPs

Oxygen sensitivity of the core–shell sensor NPs is studied by flowing a gas mixture with various N_2/O_2 ratios. As displayed in Fig. 4(A), the 645 nm emission is severely quenched with the

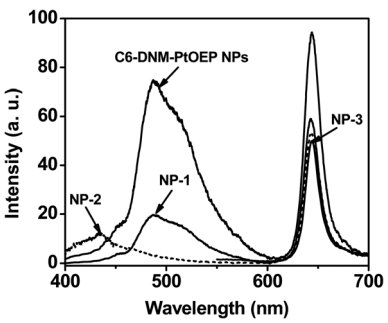

Fig. 3 Emission spectra of NPs containing C6–DNM–PtOEP, C6–PtOEP (NP-1), DNM–PtOEP (NP-2) and PtOEP (NP-3) dispersed in aqueous solution with 381 nm excitation (room temperature, air saturated).

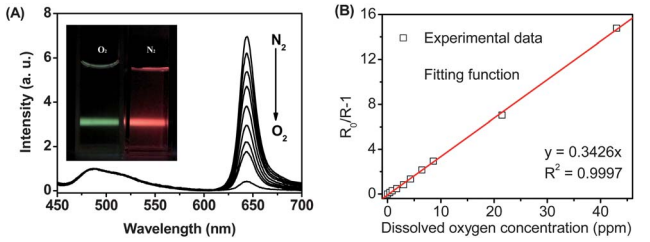

Fig. 4 Ratiometric sensing with aqueous dispersion of NPs. (A) Emission spectra under 381 nm excitation at various oxygen concentrations. From top to bottom the dissolved oxygen concentrations are 0.0 (nitrogen saturated), 0.43, 0.86, 1.72, 3.01, 4.3, 6.45, 8.6 and 43 ppm (oxygen saturated), respectively. The inset shows the photograph of the aqueous dispersion of NPs saturated with oxygen (left) and nitrogen (right) upon 381 nm illumination. (B) Stern–Volmer plot of fluorescence intensity ratios.

increase of dissolved oxygen (DO), whereas the 490 nm emission is kept constantly. The changes in the ratio of the intensities of the red and green fluorescence are visually detectable. With varying oxygen to nitrogen ratios of the purged gas, fluorescence of the aqueous dispersion of NPs switches from green to red (inset to Fig. 4(A)). This effect is quite favorable in that the ratio of the two intensities can be measured and related to the oxygen level. By defining R as the ratio of the emission intensity of PtOEP (at 645 nm) to that of C6 (at 490 nm), the sensitivity of the nanosensors can be expressed by the overall quenching response to DO,[24]

$$Q = (R_{N_2} - R_{O_2})/R_{N_2} \quad (1)$$

where R_{N_2} and R_{O_2} represent the emission intensity ratios of the sensor in fully deoxygenated and fully oxygenated solutions, respectively. The as-obtained value of Q for the hybrid sensing NPs is above 94%, which is not only much higher than normal silica-based nanosensors,[19] but also among the most sensitive polymer-based nanosensors reported so far.[18] Notwithstanding that the hydrophilic PLL-shell is disadvantageous for partitioning of dissolved oxygen into gas phase within particles, the hydrophobic core and in particular the high porosity provided by bulky phenyl groups endows the ratiometric NPs with such high sensitivity.

In bulky solid state systems, the oxygen-quenching process usually is described by the nonlinear Stern–Volmer equation due to matrix heterogeneity effects.[25] In a nanoscale system, however, the large surface/volume ratio as well as the shortened penetration depth of oxygen virtually disregards the microheterogeneity of the local environment, and oxygen quenching can be expressed, as in a homogeneous system, by the linear Stern–Volmer equation,

$$R_0/R - 1 = K_{SV}[O_2] \quad (2)$$

where R_0 is the emission intensity ratio in the absence of oxygen, R the ratio at a given oxygen concentration, K_{SV} as the Stern–Volmer quenching constant and $[O_2]$ as the DO concentration. Fig. 4(B) depicts the Stern–Volmer plot of the emission intensity ratios of NPs *versus* DO. The data fit very well over the whole range of oxygen concentration, with a correlation coefficient of

>0.999. The linear response towards oxygen is fundamental for practical oxygen sensing. It needs to be pointed out that deviations from linearity at high concentrations of oxygen have been reported in some oxygen nanosensors.[14,15] Given that the oxygen probes were incorporated into particles by polymerization, the deviations might be explained by their complicated chemical and physical environments.

2.4. Cytotoxic effect of the core–shell sensing NPs

Since the ratiometric NPs are designed for intracellular sensing, the potential cytotoxic effects are important and assessed by using an MTT assay. The MTT assay is a colorimetric assay that measures the reduction of yellow 3-(4,5-dimethythiazol-2-yl)-2,5-diphenyltetrazolium bromide (MTT) by mitochondrial succinate dehydrogenase.[26] MTT enters the cells and passes into the mitochondria where it is reduced to an insoluble colored (dark purple) formazan product. The cells are then solubilized with dimethyl sulfoxide and the released solubilised formazan reagent is measured spectrophotometrically. Therefore, it can be used to determine cytotoxicity of potential medicinal agents and toxic materials, since those agents would stimulate or inhibit cell viability and growth.

Living human hepatocellular liver carcinoma (HepG2) cells are incubated with aqueous dispersion of NPs for 12 h, and then their mitochondria and metabolic activities are examined after exposure to the complex of MTT. As shown in Fig. 5, loading of NPs with a concentration within the range from 2.9 to 14.5 μg ml^{-1} gives rise to relatively lower inhibition of cells. The low cytotoxicity of the sensing NPs is, no doubt, thanks to the biocompatible layer of PLL. In the following intracellular experiments a dosage of 11.6 μg ml^{-1} of NPs is adopted.

2.5. Stability and reversibility of the core–shell sensing NPs

The response of the ratiometric core–shell NPs towards dissolved oxygen is on the order of tens of second. It is known that dyes doped in NPs usually show improved photostability with the protection of the particle matrix. In terms of the core–shell NPs, the phosphorescence of PtOEP is bleached by ~25% under intensive continuous 381 nm illumination for 1 hour, in comparison to 80% in THF solution (Fig. 6).

It has been recently reported that silica NPs stabilized with L-lysine are not stable in physiological buffers, and even aggregated in cell culture media.[27] In contrast, the core–shell sensing NPs coated with PLL macromolecules exhibit better stability. No matter whether in buffer or culture media, no aggregate of the core–shell NPs is found. The detachment of PLL from the NPs is investigated by measuring their hydrodynamic diameters after being placed in PBS buffer solution. It is found that ~15% PLL molecules are detached from NPs after 24 h, and ~48% after 48 h (see ESI† for details). The time-dependant detachment is due to the electrostatic adsorption of PLL molecules. It should be noted that the detachment of PLL has a limited influence on both cells' viability and sensor performance, as shown by MTT assay and following intracellular imaging.

Reversibility of the ratiometric core–shell sensing NPs is tested as well. The ratio of the fluorescence intensity of PtOEP to that of C6 ($I_{F(645)}/I_{F(490)}$) was analyzed after alternate purging of the suspension of sensing NPs with N_2 and O_2 for 10 min. It could be seen clearly from Fig. 7 that the nanosensors showed complete recovery each time that the sensing environments were changed between N_2 and O_2-saturated solutions.

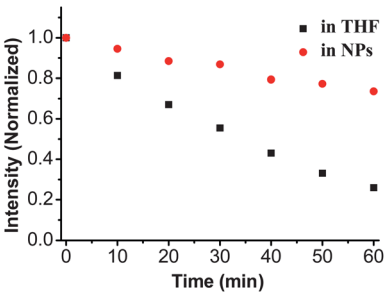

Fig. 6 Photobleaching of PtOEP in THF (square) and nanoparticles (circle). The samples were irradiated with 381 nm light at ambient atmosphere, and emission spectra were recorded every ten minutes. The intensity data were calculated from the emission peak at 645 nm.

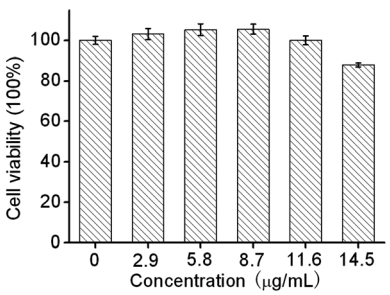

Fig. 5 HepG2 cells viability determined by MTT assay. Cells loaded with NPs at different concentrations are incubated with MTT for 4–6 hours. No significant difference between control and test groups is observed.

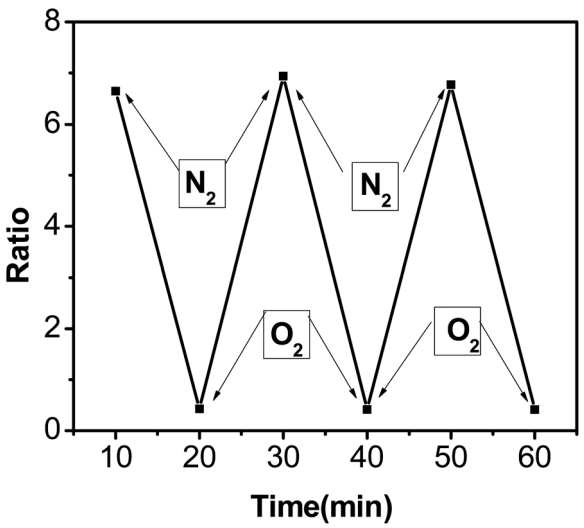

Fig. 7 Reversibility of the responsiveness of sensing NPs towards dissolved oxygen. The intensity ratios of 645 nm emission *versus* 490 nm emission under different environments are plotted against the experimental time.

2.6. Intracellular imaging of the core–shell sensing NPs

Laser confocal microscopy is used to determine the localization of the ratiometric sensing NPs inside HepG2 cells, as shown in Fig. 8. A comparison of the differential interference contrast (DIC) image and fluorescence images of the cells clearly indicates that a good fraction of the NPs has been actively incorporated, presumably by vesicular uptake mechanisms. The strong cellular uptake further demonstrates that the core–shell NPs are stable enough for intracellular experiments. The NPs are localized inside the cytoplasm without penetrating into the nucleus. The inhomogeneous distribution of particles indicates an accumulation in intracellular organelles, such as the endoplasmic reticulum or the Golgi apparatus. Fluorescence of the reference C6 (Fig. 8(b)) and probe PtOEP (Fig. 8(c)) is recorded with single-wavelength excitation and separate emission filters. The perfect co-localization of the dual fluorescence suggests that intracellular oxygen sensing with the ratiometric nanosensors is possible.

3. Experimental

3.1. Materials

Coumarin 6, platinum(II) octaethylporphine (PtOEP), polystyrene (PS, M_w = 280 kDa), poly-L-lysine (PLL, M_w = 4–15 kDa) and THF were purchased from Sigma-Aldrich. Dodecyltrimethoxysilane (DTS) was from Jiaxing Sicheng Chemicals Co., Ltd (China). All chemicals were used without further purification. Dinaphthoylmethane (DNM) was synthesized according the procedures described in ref. 16. Doubly distilled water was used in all experiments.

3.2. Synthesis of core–shell sensing NPs

In a typical experiment, PtOEP, C6, DNM, PS and DTS were dissolved in THF, in a 1 : 3 : 3 : 43 : 50 weight ratio and at a total concentration of 200 ppm. Then under sonication, 500 μl of the solution were rapidly injected, using a microsyringe, into 8 ml basic water (pH 9, adjusted by addition of ammonium hydroxide) containing 0.16 mg PLL. The resulting suspensions were left standing for 2 h, and then dialysed against water for 24 h. The resulting suspension (containing around 29 mg of NPs per liter) was stored at 4 °C for further experiments including spectral characterization, SEM, TEM, zeta potential, test of oxygen sensitivity, cell incubations and confocal microscopy measurements.

The concentration of doped dyes in NPs can be tuned by increasing or decreasing the concentration of PS, whilst kept the fraction of DTS at 50%. As the ratio of the probe to reference should be of comparable emission intensity at ambient atmosphere, the doping ratio of PtOEP–C6–DNM in NPs is empirically determined to be best at 1, 3 and 3 wt%.

3.3. Characterization

TEM images were obtained with an electron microscope (type Hitachi H-800) at an acceleration voltage of 200 kV. SEM images were done on a field emission scanning electron microscope (JEOL JSM-7500F), using aqueous dispersion of NPs placed on the SEM specimen support (aluminum), subsequently evaporated at room temperature and sputter coated with Au. Zeta potentials were determined by photon correlation spectroscopy using a Zetasizer Nano instrument (Malvern Instruments, Malvern, UK). The measurements were performed at 25 °C with a detection angle of 90°. UV-visible absorption spectra and steady-state fluorescence spectra were recorded on a UV-3101PC spectrophotometer (Shimadzu) and an F-4500 fluorescence spectrophotometer (Hitachi), respectively.

3.4. Oxygen calibration, reversibility test and experimental setup

The calibration and reversibility were both carried out in a cell placed with 2 ml of NP solution. The cell was sealed with Parafilm (Chicago, IL, USA), through which two 1.5 inch needles were used as gas inlet and outlet ports. Different dissolved oxygen (DO) concentrations were obtained by flowing O_2–N_2 gas mixture with various ratios, controlled by a WITT gas mixer (type KM60-2, www.wittgas.com, Germany) in the range of 1–25% with an accuracy of 1% absolute. In addition, two high DO concentrations were realized by directly flowing a mixture of N_2–O_2 (50/50) and O_2 respectively. All spectra measurements were performed at room temperature. The DO concentrations in NP solutions were deduced according to that in oxygen-saturated solutions (43 ppm) based on the solubility equation of oxygen in water. For the reversibility experiments, nitrogen and oxygen gases were alternately flowed into the cell over 10 minutes.

3.5. Cells culture and MTT assay

HepG2 cells were grown in 6 cm cell glass-bottom culture dishes in RPMI-1640 cell medium supplemented with 10% FBS at 37 °C under humid conditions with CO_2 (5%).

For MTT assay, HepG2 cells were seeded on a 96-well microtiter plate at approximate 5×10^3 cells per well, and

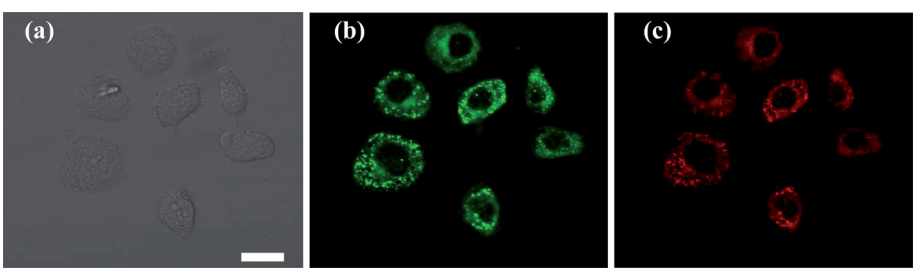

Fig. 8 DIC (a) and confocal fluorescence images (b and c) of HepG2 cells loaded with 11.6 μg ml^{-1} of sensing NPs (air atmosphere). The scale bar is 20 μm. The green (C6) and red (PtOEP) fluorescence were, respectively, collected at 475–550 and 620–680 nm with a 458 nm excitation wavelength.

incubated 12 h to allow the cells to attach the well. The 96 wells were classified into six groups, with one group left for blank control. NPs aqueous dispersions were sterilized by UV illumination for 10 minutes before loading. Then 20, 40, 60, 80 and 100 μl of NP suspension were in sequence added into respective wells, whilst the total volume was kept constantly at 200 μl by decreasing the quantity of culture medium. After incubation for 12 h, 10 μl of 3-(4,5-dimethylthiazol-2-yl)-2,5-diphenyltetrazolium bromide (MTT, 5 mg ml^{-1} in PBS solution, pH 7.4) was added into each well. The microtiter plate was further incubated for 4 h to allow MTT to be metabolized. Then the mixed solution was drained off and formazan (MTT metabolic product) was dissolved by adding 100 μl per well dimethyl sulfoxide (DMSO). After being shaken for 5 minutes, optical density (OD) was measured spectrophotometrically in an ELISA reader (BioTek, ELx800™) at a wavelength of 490 nm (test) and 630 nm (reference). The relative cell viability (%) related to control wells containing cell culture medium without NPs was calculated by OD (test)/OD (control) × 100.

3.6. Live confocal microscopy imaging

HepG2 cells (1×10^5) were first seeded in a 35 mm confocal culture dish with 2 ml LRPMI-1640 supplemented with 10% fetal bovine serum (FBS). After 12 h incubation, the cell media were replaced with 1.2 ml of fresh culture media and 0.8 ml of sterilized NP suspension, and allowed to incubate for another 12 h. Afterwards the cells were washed three times with PBS before microscopy viewing.

Intracellular imaging was conducted on an Olympus FV1000 confocal laser scanning microscopy. Acquisition of each spectral signal was done in Kalman laser mode. The ratiometric NPs were excited at 458 nm (48% of laser power) with emission collected at 475–550 nm and at 620–680 nm, respectively. In all the experiments, fluorescent and differential interference contrast (DIC) images were collected with a 40× immersion objective using 0.5 μm steps. The resulting *z*-stacked images were analyzed using FV1000 Viewer (Olympus).

4. Conclusions

In summary, we report a novel ratiometric biocompatible core–shell oxygen nanosensor. Based on intraparticle FRET, the NPs constructed from a spectrally non-matched dual-dye system give dual emission with single-wavelength excitation. Such a strategy is expected to enrich the category of ratiometric nanosensor, not limited for oxygen. Moreover, PLL molecules are coated *in situ* by the facile ER method, resulting in core–shell NPs. The positively charged biocompatible shell gives the nanosensors low cytotoxic effects as well as effortless cellular uptake. Most importantly, the surface amino groups provided by PLL molecules enable further conjugation with a wide range of biomolecules. These ratiometric sensing NPs are proved to be highly sensitive to dissolved oxygen, and intracellular oxygen sensing is very promising.

Acknowledgements

The work was supported by NSF of China (grant no. 61078069, 10874014 and 10979009), NSF for Distinguished Young Scholars (61125505) and Fundamental Research Funds for the Central Universities (2010JBZ006).

Notes and references

1 M. Höckel, K. Schlenger, S. Hockel, B. Aral, U. Schaffer and P. Vaupel, *Int. J. Cancer*, 1998, **79**, 365.
2 J. Lopez-Barneo, R. Pardal and P. Ortega-Saenz, *Annu. Rev. Physiol.*, 2001, **63**, 259.
3 S. M. Evans and C. J. Koch, *Cancer Lett.*, 2003, **195**, 1.
4 T. Acker and H. Acker, *J. Exp. Biol.*, 2004, **207**, 3171.
5 J. N. Demas and B. A. DeGraff, *Coord. Chem. Rev.*, 2001, **211**, 317–351.
6 Y. Amao, *Microchim. Acta*, 2003, **143**, 1.
7 A. Fercher, T. C. O'Riordan, A. V. Zhdanov, R. I. Dmitriev and D. B. Papkovsky, *Methods Mol. Biol.*, 2010, **591**, 257–273.
8 A. Fercher, S. M. Borisov, A. V. Zhdanov, I. Klimant and D. B. Papkovsky, *ACS Nano*, 2011, **5**, 5499.
9 M. S. Tremblay, M. Halim and D. Sames, *J. Am. Chem. Soc.*, 2007, **129**, 7570.
10 G. Zhang, G. M. Palmer, M. W. Dewhirst and C. L. Fraser, *Nat. Mater.*, 2009, **8**, 747.
11 X. D. Wang, Xi. Chen, Z. X. Xie and X. R. Wang, *Angew. Chem., Int. Ed.*, 2008, **47**, 7450.
12 X. D. Wang, R. J. Meier, M. Link and O. S. Wolfbeis, *Angew. Chem., Int. Ed.*, 2010, **49**, 4907.
13 X. D. Wang, T. Y. Zhou, X. H. Song, Y. Jiang, C. J. Yang and X. Chen, *J. Mater. Chem.*, 2011, **21**, 17651.
14 S. H. Im, G. E. Khalil, J. Callis, B. H. Ahn, M. Gouterman and Y. Xia, *Talanta*, 2005, **67**, 492.
15 Y. E. K. Lee, E. E. Ulbrich, G. Kim, H. Hah, C. Strollo, W. Fan, R. Gurjar, S. Koo and R. Kopelman, *Anal. Chem.*, 2010, **82**, 8446.
16 X. D. Wang, H. H. Gorris, J. A. Stolwijk, R. J. Meier, D. B. M. Groegel, J. Wegener and O. S. Wolfbeis, *Chem. Sci.*, 2011, **2**, 901.
17 Y. E. L. Koo, Y. Cao, R. Kopelman, S. M. Koo, M. Brasuel and M. A. Philbert, *Anal. Chem.*, 2004, **76**, 2498.
18 C. F. Wu, B. Bull, K. Christensen and J. McNeill, *Angew. Chem., Int. Ed.*, 2009, **48**, 2741.
19 H. Xu, J. W. Aylott, R. Kopelman, T. J. Miller and M. A. Philbert, *Anal. Chem.*, 2001, **73**, 4124.
20 H. S. Peng, C. F. Wu, Y. F. Jiang, S. H. Huang and J. McNeill, *Langmuir*, 2007, **23**, 1591.
21 H. S. Peng, M. I. J. Stich, J. B. Yu, L. N. Sun, L. H. Fischer and O. S. Wolfbeis, *Adv. Mater.*, 2010, **22**, 716.
22 G. L. Kenausis, J. Vörös, D. L. Elbert, N. Huang, R. Hofer, L. R. Taylor, M. Textor, J. A. Hubbell and N. D. Spencer, *J. Phys. Chem. B*, 2000, **104**, 3298.
23 M. D. McGehee, T. Bergstedt, C. Zhang, A. P. Saab, M. B. O'Regan, G. C. Bazan, V. I. Srdanov and A. J. Heeger, *Adv. Mater.*, 1999, **11**, 1349.
24 C. McDonagh, B. D. MacCraith and A. K. McEvoy, *Anal. Chem.*, 1998, **70**, 45.
25 (*a*) S. Draxler and M. E. Lippitsch, *Anal. Chem.*, 1996, **68**, 753; (*b*) P. Hartmann and W. Trettnak, *Anal. Chem.*, 1996, **68**, 2615.
26 T. Mosmann, *J. Immunol. Methods*, 1983, **65**, 55.
27 C. Graf, Q. Gao, I. Schütz, C. N. Noufele, W. Ruan, U. Posselt, E. Korotianskiy, D. Nordmeyer, F. Rancan, S. Hadam, A. Vogt, J. Lademann, V. Haucke and E. Rühl, *Langmuir*, 2012, **28**, 7598.